J Mater Sci (2006) 41:4948–4960
DOI 10.1007/s10853-006-0032-9

Formation of boride layers at the Fe–25% Cr alloy–boron interface

V. I. Dybkov · W. Lengauer · P. Gas

Received: 21 April 2005 / Accepted: 22 September 2005 / Published online: 9 May 2006

Abstract Two boride layers based on the FeB and Fe_2B compounds are formed at the interface between a Fe–25% Cr alloy and boron at 850–950 °C and reaction times up to 12 h. The characteristic feature of both layers is a pronounced texture. Each of two boride layers is compositionally two-phase. The outer layer consists of the (Fe,Cr)B and (Cr,Fe)B phases. The inner layer comprises the $(Fe,Cr)_2B$ and $(Cr,Fe)_2B$ phases. The diffusional layer-growth kinetics are close to parabolic and can alternatively be described by a system of two non-linear differential equations, also producing a fairly good fit to the experimental data. Annealing of a borided Fe–Cr sample in the absence of boriding media results in the disappearance of the (Fe,Cr)B–(Cr,Fe)B layer, with the (Fe,Cr)B phase disappearing first. Microhardness values are 21.0 GPa for the outer layer, 18.0 GPa for the inner layer and 1.35 GPa for the alloy base. The abrasive wear resistance of the (Fe,Cr)B–(Cr,Fe)B layer, found from mass loss measurements, is more than 150 times greater than that of the alloy base.

V. I. Dybkov (✉)
Department of Physical Chemistry of Inorganic Materials, Institute for Problems of Materials Science, Kyiv 03180, Ukraine
e-mail: vdybkov@ukr.net

W. Lengauer
Institute for Chemical Technologies and Analytics, Vienna University of Technology, 1060 Vienna, Austria

P. Gas
L2MP-CNRS, Faculté des Sciences St Jerome, Case 142, 13397 Marseille, France

Introduction

Boriding is one of the widespread thermochemical surface treatments used to improve service characteristics (hardness, mechanical and corrosive wear resistance, etc.) of steels, metals and alloys [1–3]. Iron borides Fe_2B and FeB are known to exist in the Fe–B binary system [4–7]. Therefore, with iron, its alloys and steels, either one-phase or two-phase coatings can be obtained, depending on boriding techniques employed and temperature-time conditions of a boriding procedure.

It is worth mentioning that even if three or more compounds exist in the metal–boron binary system, in most cases only two of them form separate layers at the interface between reacting phases [8]. This contradicts diffusional considerations [9] predicting the simultaneous formation and subsequent parabolic growth of the layers of all compounds of any binary system, whatever their number, but agrees with a physicochemical viewpoint [10], according to which one or two layers can occur and grow simultaneously under conditions of diffusion control, with other compound layers being skipped for kinetic reasons.

The properties of boride coatings are to a large extent dependent on the amount of alloying elements and impurities present in the base material. In the case of materials of complicated chemical composition, for example steels, it is not so easy to separate the effect of a particular element from that of others. Therefore, experiments with binary alloys are desirable. In this work, the results of the experimental investigation of the interaction of an Fe–25%Cr alloy with boron at 850–950 °C are presented.

Experimental procedure

Materials and specimens

The materials used were high-purity carbonyl iron powder (99.98% Fe), electrolytic-grade chromium plateletes (99.98% Cr), amorphous boron and analytical-grade KBF_4. Initially, the boron powder contained 98.3% B, 0.04% C, 1.6% O and insignificant amounts of Si, Cu, Mg ($<0.01\%$ each) and Fe ($<0.001\%$). Before the boriding experiments, the powder was first heated slowly in vacuum up to 1450 °C and then calcined at this temperature for 2 h in an atmosphere of argon at a pressure of 2.5×10^4 Pa to remove volatile oxides. KBF_4 was preliminary dried in steps at 95, 110, 130 and 170 °C (24 h at each temperature).

Cylindrical rods of an Fe–25% Cr alloy, about 13 mm in diameter and 100 mm long, were prepared by arc-melting of appropriate metals under argon, with subsequent casting of the melts into water-cooled copper crucibles. The rods were annealed to ensure their homogenization at a temperature of 1100 °C for 2 h in an argon atmosphere at a pressure of 2.5×10^4 Pa. From these, Fe–Cr alloy specimens in the form of tablets, 11.28 mm diameter and 5.5 mm high, were machined. Flat sides (1 cm^2 area) of the tablets were ground and polished mechanically.

Methods

The boriding procedure was performed using a vacuum device VPBD-2S consisting of a high-vacuum chamber with a molybdenum-sheet electric-resistance furnace (temperatures up to 1600 °C) and a control panel. The experiment was carried out in an alumina crucible, 13 mm inner diameter and 40 mm high. An iron–chromium alloy tablet was embedded into a mixture of boron powder with 5% KBF_4 as an activator. This amount of KBF_4 appears to be optimum [1, 8]. The mixture was then slightly pressed, and a load of 8.5 g (a low-carbon steel cylinder) was placed on top. The crucible was closed with a low-carbon steel lid and placed into a steel-sheet holder, mounted to a guide rod capable of moving in the vertical direction.

The chamber was pumped to a pressure of about 10 Pa and filled with high-purity argon (99.999 vol.% Ar). This procedure was repeated twice. Then, the chamber was again pumped and filled with argon at a pressure of 2.5×10^4 Pa, and heating was started. During heating, the crucible with its contents was in the cold zone above the furnace.

After the required temperature in the range of 850–950 °C had been reached in the furnace, the crucible, preheated to about 400 °C, was moved into its middle part. After an initial drop, the temperature attained its predetermined value in 4–5 min and was then maintained constant within ±1 °C with the help of an automatic thermoregulator VRT-3. The temperature measurements were carried out using a Pt–PtRh thermocouple. The experiments were carried out at temperatures of 850, 900 and 950 °C. Their duration was 3,600–43,200 s (1–12 h).

After the experiment, the Fe–Cr alloy tablet coated with boride layers was cut along the cylindrical axis into two unequal parts (7 mm and 4 mm) using an electric-spark machine. The greater part of the tablet was embedded into a cold-setting epoxy resin and used to prepare a metallographic cross-section. The lesser part was used for X-ray diffraction investigations (plain-view samples).

Characterization of Fe–Cr alloys and boride layers was carried out with the help of metallography, X-ray (XA) and chemical (CA) analyses, and electron probe microanalysis (EPMA). The composition of the Fe–Cr alloy prepared was found by CA and EPMA to correspond to a nominal value of 25% Cr within ±0.4%. Its constituting phase was shown by XA to be the α-phase.

The thickness of boride layers was measured using an optical microscope MIM-7 equipped with a HP Photosmart 720 camera. The chemical composition of the layers and the concentration profiles of the elements in the transition zone between reacting phases were obtained using electron probe microanalyzers JEOL Superprobe 733 and CAMECA Camebax SX50. The beam spot diameter and the phase volume analyzed at each point were estimated to be about 1 μm and 2 μm^3, respectively.

X-ray diffraction patterns were taken immediately from the surface of tablet samples on a DRON-3 apparatus using CuK_α radiation. When taking the first pattern, no polishing of a borided Fe–Cr alloy sample was applied (section 0). Then, about 10 μm of a boride layer was removed by grinding and subsequent polishing, and another X-ray diffraction pattern was taken (section I). This procedure was repeated at a step of 10–40 μm until the Fe–Cr alloy base was reached (sections II–VI). Seven X-ray diffraction patterns were thus taken on each borided Fe–Cr sample.

Microhardness measurements on metallographic cross-sections were carried out using a PMT-3 tester with the diamond pyramide. The load was 0.98 N (100 g).

Abrasive wear resistance tests were carried out on P180 silicon carbide emery paper tape (main fraction grain size 63 μm, maximum 90 μm) using an AWRD-5 device. The velocity of continuous movement of the tape (30 m long) was 0.35 m s^{-1}, while the sliding distance during each test was 27.0 m. The load was 50 N (5.1 kg). The working area of tablet samples was 1 cm^2. The wear resistance of boride layers and the alloy base was determined by means of weighing the samples and measuring their height.

Results and discussion

Phase identity and chemical composition of boride layers

Two boride phases were found to occur as separate layers at the interface between an Fe–25% Cr alloy and boron at 850–950 °C and reaction times up to 12 h, as illustrated in Fig. 1. Layer-by-layer X-ray diffraction analysis (Fig. 2) and a further comparison of our and literature [11] data showed the outer layer bordering the boriding agent to be the FeB phase and the inner layer adjacent to the Fe–Cr alloy base to be the Fe_2B phase (Fig.3 and Tables 1 and 2).

As seen from cross-sectional micrographs in Figs. 1 and 2, both layers consist of columnar crystals oriented preferentially in the direction of diffusion or at an angle of 20°–25° to this direction. Their characteristic feature is a pronounced texture. The strongest reflections are {002} ($2\theta = 63.4^{o}$ and spacing, $d = 0.148$ nm) and, to a lesser extent, {020} ($2\theta = 32.5^{o}$ and $d = 0.275$ nm) for the orthorhombic FeB phase, and {002} ($2\theta = 42.8^{o}$ and $d = 0.212$ nm) for the tetragonal Fe_2B phase, in agreement with findings of other researchers [1, 12–14]. The change in intensities of those reflections with increasing distance from the surface of a borided Fe–25% Cr alloy tablet is shown in Fig.4 and Table 3.

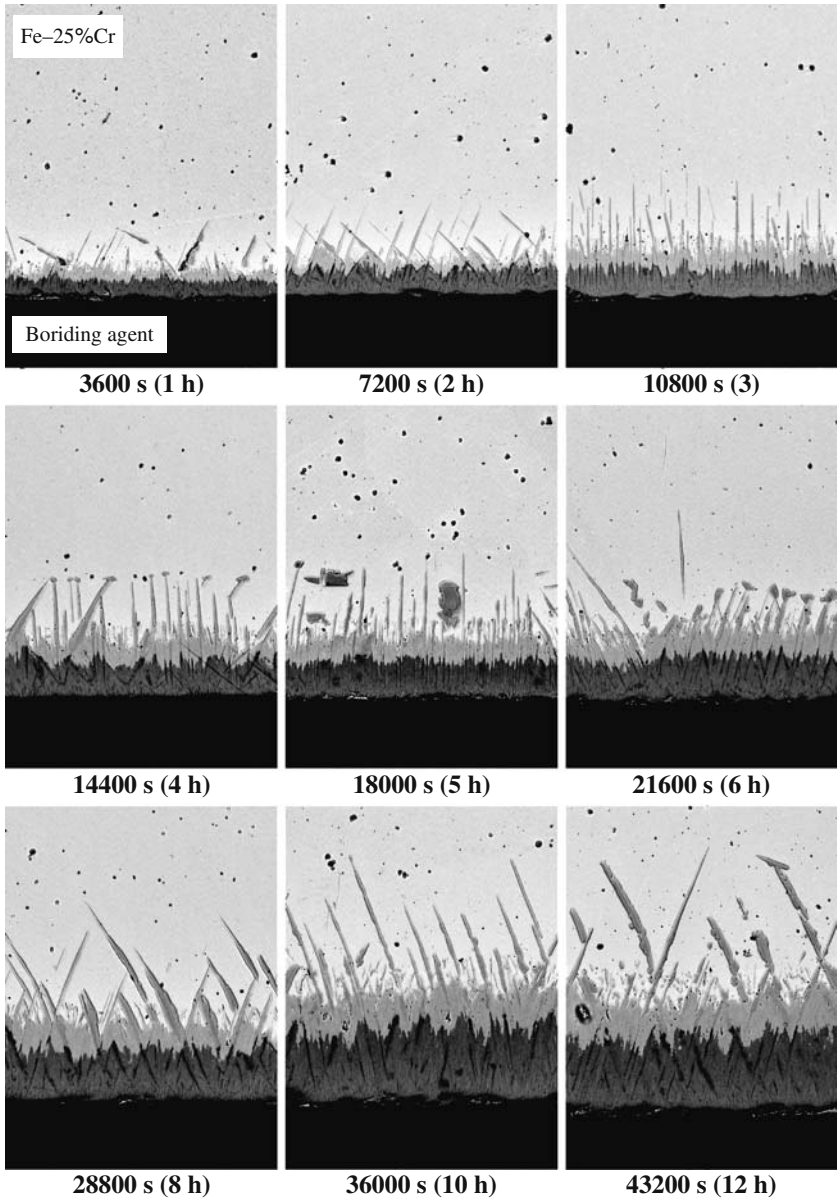

Fig. 1 Backscattered electron images of boride layers formed at the Fe–25% Cr alloy–boron interface at a temperature of 950 °C. Layer-by-layer X-ray analysis showed the darker layer bordering the boriding agent to be the FeB phase and the brighter layer adjacent to the Fe–Cr alloy base to be the Fe_2B phase

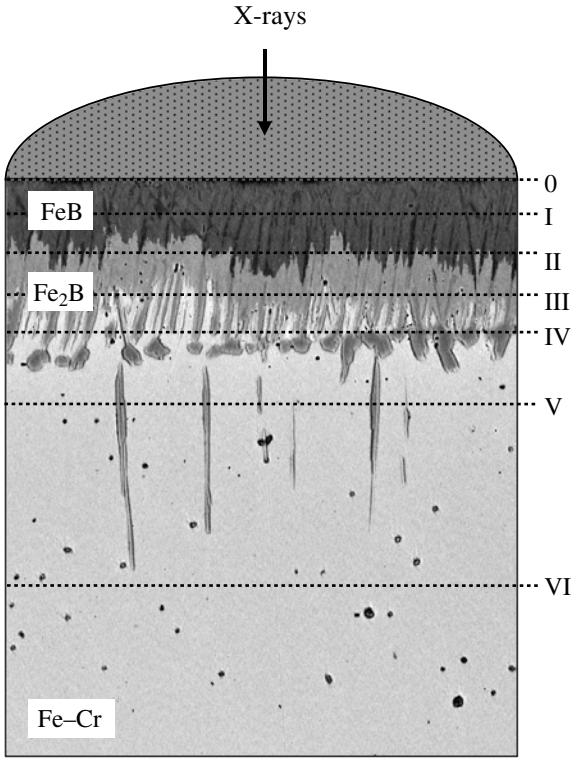

Fig. 2 Scheme of X-ray diffraction experiments

As evidenced in Fig.4 and Table 3 (see also Fig. 2), the larger orientation order (higher peak intensity) is characteristic of the inner portions of both boride layers compared to their near-interface portions. This is easily explainable because near-interface portions of any boride layer are less equilibrated compared to its inner portions. Therefore, near-interface crystals have less time to align in the preferred direction. The boride layer ordering process has been considered in detail by Voroshnin and Lyakhovich [1] and recently by Martini et al. [14] (see Fig. 3 of their paper).

X-ray investigations were followed by EPMA measurements (Table 4). Sections 0 and I of a borided Fe–Cr sample seem to correspond to a single-phase region (see Fig. 2). However, even though with iron, its alloys and steels a boride layer bordering the boriding agent is conventionally considered to consist of the FeB phase [1] and our X-ray diffraction data provide the strong support to this view-point, its microstructure (Fig. 5) and chemical composition (Table 4) is in fact more complicated. As seen from plain-view micrographs of Fig. 5, the outer boride layer consists of distinct brighter and darker regions, with the latter having a peculiar regular arrangement. EPMA measurements in Table 4 indicate that iron prevails in brighter regions, while chromium is dominant in darker regions.

Hence, compositionally the outer boride layer actually comprises the (Fe,Cr)B and (Cr,Fe)B phases, although X-ray diffraction analysis does not show the presence of the CrB phase, probably because, firstly, the FeB and CrB phases have very similar crystal structures [4–6, 11] and, secondly, under non-equilibrium conditions the lattice rearrangement is not completed in view of time limitations. Being far from equilibrium, this layer appears to be single-phase structurally and two-phase compositionally. Since the scan line in Fig. 6 crosses areas of different chemical composition (even within the same boride phase), it is not surprising that the cross-sectional con-

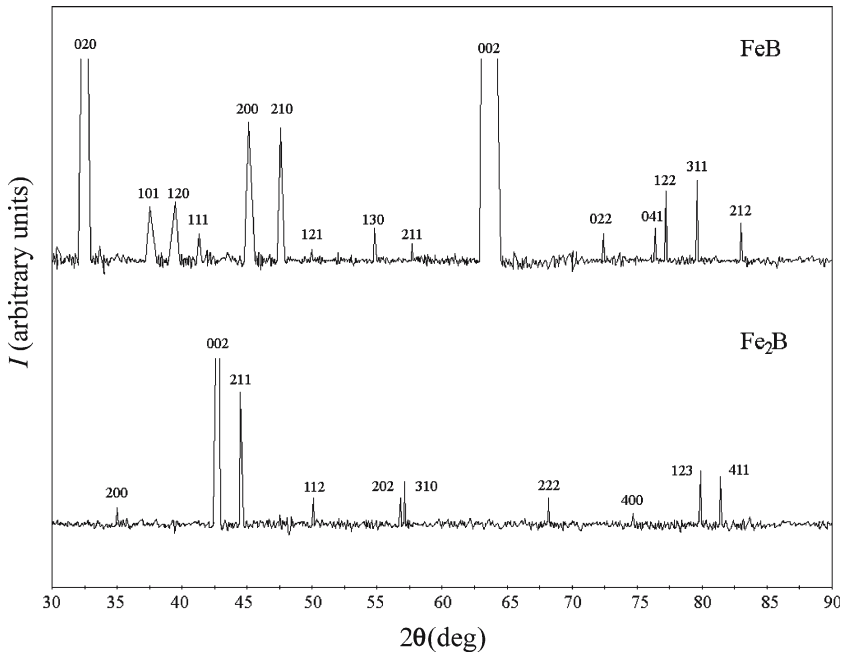

Fig. 3 X-ray diffraction patterns of the FeB and Fe_2B phases. Boriding conditions: temperature 950 °C, reaction time 21,600 s (6 h)

Table 1 Comparison of literature and our experimental X-ray data (*d*-spacing and peak intensities) for the FeB phase formed at the interface between an Fe–25% Cr alloy and boron at 950 °C and a reaction time of 21600 s (6 h)

Literature data [11]			Experimental data		
HKL	*d* (nm)	*I*[a]	2θ (deg)	*d* (nm)	*I*
020	0.275	s	32.5	0.2752	vs
101	0.240	s	37.3	0.2410	m
120	0.228	s	39.5	0.2281	m
111	0.219	vs	41.3	0.2186	w
200; 021	0.201	vs	45.1	0.2010	vs
210	0.190	vs	47.6	0.1910	s
121	0.181	s	50.0	0.1811	vw
130	0.167	s	54.8	0.1675	w
211	0.160	s	57.7	0.1597	vw
002	0.148	m	63.4	0.1467	vs
022	0.1303	m	72.4	0.1305	w
041	0.1249	m	76.4	0.1246	w
122	0.1239	vs	77.2	0.1236	m
311	0.1199	m	79.6	0.1204	m
212	0.1166	vs	83.0	0.1163	w

[a]Intensity: vw, very weak; w, weak; m, medium; s, strong; vs, very strong

Table 2 Comparison of literature and our experimental X-ray data (*d*-spacing and peak intensities) for the Fe_2B phase formed at the interface between an Fe–25% Cr alloy and boron at 950 °C and a reaction time of 21600 s (6 h)

Literature data [11]			Experimental data		
HKL	*d* (nm)	*I*[a]	2θ (deg)	*d* (nm)	*I*
200	0.256	vw	35.0	0.2549	vw
002	0.212	w	42.8	0.2113	vs
211	0.201	vs	44.5	0.2014	vs
112	0.183	m	50.1	0.1831	w
202	0.163	m	56.8	0.1628	w
310	0.161	m	57.1	0.1615	m
222	0.1371	w	68.2	0.1375	w
400	0.1277	m	74.7	0.1272	vw
123	0.1202	s	79.9	0.1199	m
411	0.1187	m	81.4	0.1182	m

[a]Intensity: vw, very weak; w, weak; m, medium; s, strong; vs, very strong

centration profiles of the elements Fe, Cr and B are so irregular, except iron and chromium profiles in the alloy base.

As seen in Fig. 2 and Table 3, section II crossed both the FeB and Fe_2B layers, whereas section III crossed the Fe_2B layer and partially the alloy base. The Fe_2B layer was also found to be non-homogeneous (Fig. 7). Like the FeB layer, it consists of the $(Fe,Cr)_2B$ phase (region **A** in Fig. 7, see also Table 4) and the $(Cr,Fe)_2B$ phase (region **B**). Note that the Fe_2B and Cr_2B phases are isomorphous [4–6, 11].

The microstructure of sections IV and V consists of the $(Cr,Fe)_2B$ phase in the decreasing amount and the alloy base somewhat depleted in chromium (Fig. 8 and Table 4). Section VI is entirely the alloy base of an initial composition of 25% Cr.

Microhardness of boride phases

Microhardness, HV_{100}, of the outer (Fe,Cr)B–(Cr,Fe)B layer was found to be 21.0 ± 2.0 GPa, while that of the inner $(Fe,Cr)_2B$–$(Cr,Fe)_2B$ layer to be 18.0 ± 1.0 GPa. For the Fe–25% Cr alloy base, its value is 1.35 ± 0.09 GPa.

Microhardness values vary considerably within both boride layers in view of their non-homogeneity. The difference in microhardness of near-boride and far-away Fe–Cr regions is insignificant (about 0.1 GPa).

Layer-growth kinetics

Even though the boride layers are rather irregular, it is possible to extract some kinetic data from the experimental results obtained. With the ragged inner boride layer, the

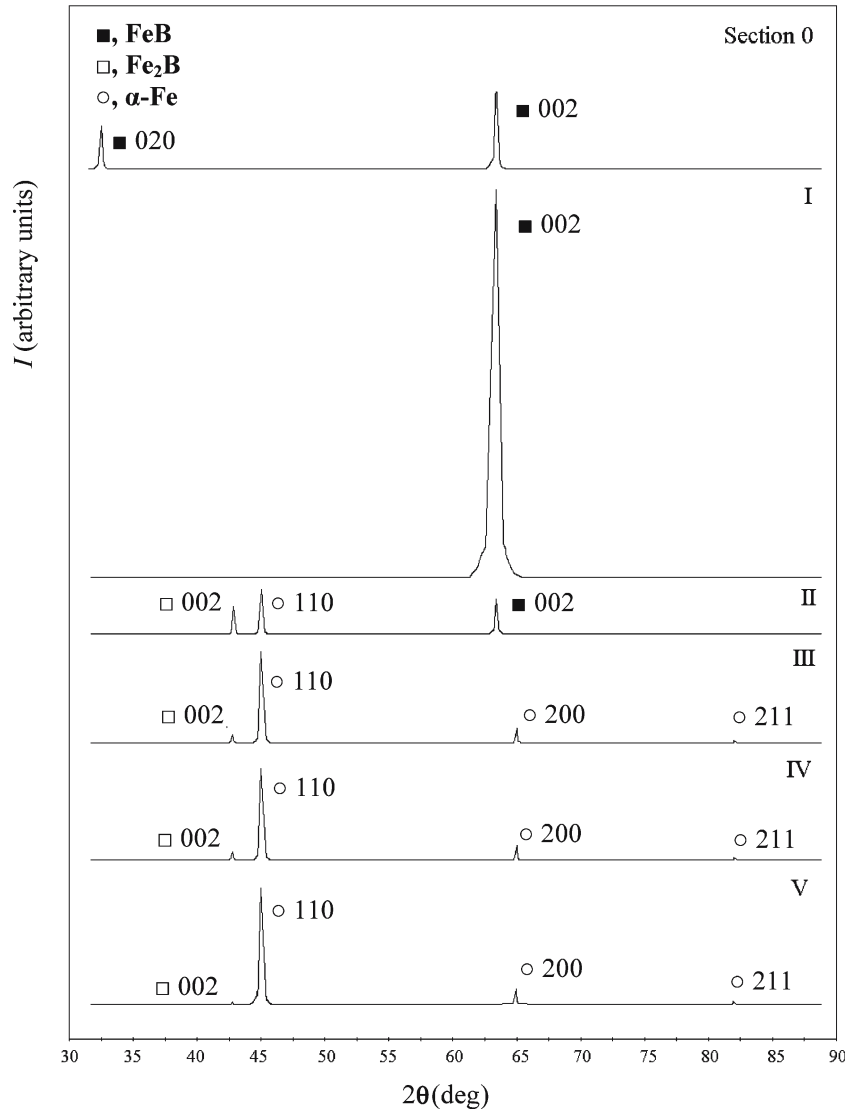

Fig. 4 Most intensive peaks of X-ray diffraction patterns taken from different plain-view sections of an Fe–25% Cr alloy sample borided at 950 °C for 21600 s (6 h) (see also Fig. 2 and Table 3)

Table 3 X-ray diffraction data showing preferential directions of growth for the FeB and Fe_2B phases formed at the interface between an Fe–25% Cr alloy and boron at 950 °C and a reaction time of 21600 s (6 h) (see also Figs. 1, 2)

Phase	*HKL*	*d* (nm)	Peak intensity (arbitrary units)					
			0[a]	I	II	III	IV	V
FeB	020	0.275	90					
	002	0.148	161	650	77			
Fe_2B	002	0.212			65	33	28	10
α-Fe	110	0.201			92	168	185	195
	200	0.143				43	95	97
	211	0.117				24	31	32

[a]Serial numbers of appropriate sections of a borided tablet sample by a plane parallel to its flat surface (section 0, I, II and so on, deeper into the sample bulk, see Fig. 2)

continuous front thickness was measured, while the separate long crystals of the $(Cr,Fe)_2B$ phase penetrating deep into the alloy base were neglected.

It should be noted that, due to a variety of boriding media employed, kinetic data of different authors differ considerably, even for similar alloys or steels. For example, Goeuriot et al. [12] reported that a compact boride layer, 5 μm thick, is formed on the surface of a 26% Cr–1% Mn steel sample, borided in activated B_4C powder at 950 °C for 4 h, with separate fine boride needles extending to

Table 4 Fe, Cr and B contents of reacting phases, found by EPMA measurements on X-ray diffraction samples (see also Figs. 2, 3, 5, 6)

Section in Fig. 2	Region	Content (at.%)			Phase
		Fe	Cr	B	
I	Brighter in Fig. 3	25.9	23.9	50.2	(Fe,Cr)B
		29.0	22.9	48.1	
		26.9	21.1	52.0	
		29.2	19.9	50.9	
		33.1	16.2	50.7	
	Darker in Fig. 3	23.7	24.4	51.9	(Cr,Fe)B
		22.0	29.5	48.5	
		17.7	32.2	50.1	
		20.9	29.8	49.2	
		15.0	33.1	51.9	
III	**a** in Fig. 5	56.6	12.2	31.2	$(Fe,Cr)_2B$
		53.9	11.5	34.6	
		50.0	16.2	33.8	
	b in Fig. 5	18.4	46.8	34.8	$(Cr,Fe)_2B$
		24.2	44.1	31.7	
		19.6	46.8	33.6	
	c in Fig. 5	79.4	20.6	0.0	Fe–Cr
		77.5	22.5	0.0	
		81.9	18.1	0.0	
IV	Brighter in Fig. 6	76.1	23.9	0.0	Fe–Cr
		80.1	19.4	0.5	
		74.2	25.8	0.0	
	Darker in Fig. 6	18.8	49.2	32.1	$(Cr,Fe)_2B$
		19.0	47.0	34.0	
		19.6	50.7	29.7	
V	Brighter in Fig. 6	72.8	27.2	0.0	Fe–Cr
		72.2	27.8	0.0	
		72.5	27.5	0.0	
	Darker in Fig. 6	23.4	43.1	33.5	$(Cr,Fe)_2B$
		18.6	48.7	32.7	
		21.8	45.1	33.1	
VI		73.9	26.1	0.0	Fe–25%Cr
		73.0	27.0	0.0	
		73.7	26.3	0.0	

about 50 μm into the steel matrix. In our investigation, appropriate values for the Fe–25% Cr alloy are 65 μm and around 120 μm. This great difference appears to arise mainly from the different potential of boriding agents rather than from the difference in the chemical composition of those materials.

The growth kinetics of two compound layers are usually treated using parabolic equations of the type $x^2 = 2k_1t$, where x is the layer thickness, k_1 is the layer growth-rate constant and t is time [9, 15, 16]. As seen in Fig. 9 and Table 5, such equations produce a quite satisfactory fit to the experimental data obtained. The average values of layer growth-rate constants are presented in Table 6.

In fact, however, growth kinetics of the FeB and Fe_2B layers at the diffusional stage of their formation are somewhat more complicated and may alternatively be described by a system of two non-linear equations [10, 17]

$$\frac{dx}{dt} = \frac{k_{outer}}{x} - \frac{rg}{p}\frac{k_{inner}}{y} \tag{1a}$$

$$\frac{dy}{dt} = \frac{k_{inner}}{y} - \frac{q}{sg}\frac{k_{outer}}{x} \tag{1b}$$

where x is the FeB layer thickness, y is the Fe_2B layer thickness, k_{outer} is the FeB layer growth-rate constant, k_{inner} is the Fe_2B layer growth-rate constant, g is the ratio of the molar volumes of the FeB and Fe_2B compounds, $p = q = r = 1$ and $s = 2$ (factors from the chemical formulae of FeB and Fe_2B).

An obvious criterion for the applicability of the system of equations 1 is the constancy of k_{outer} and k_{inner} over a given range of time, as is the case with both boride layers (Tables 5 and 6). The value of g necessary for calculations

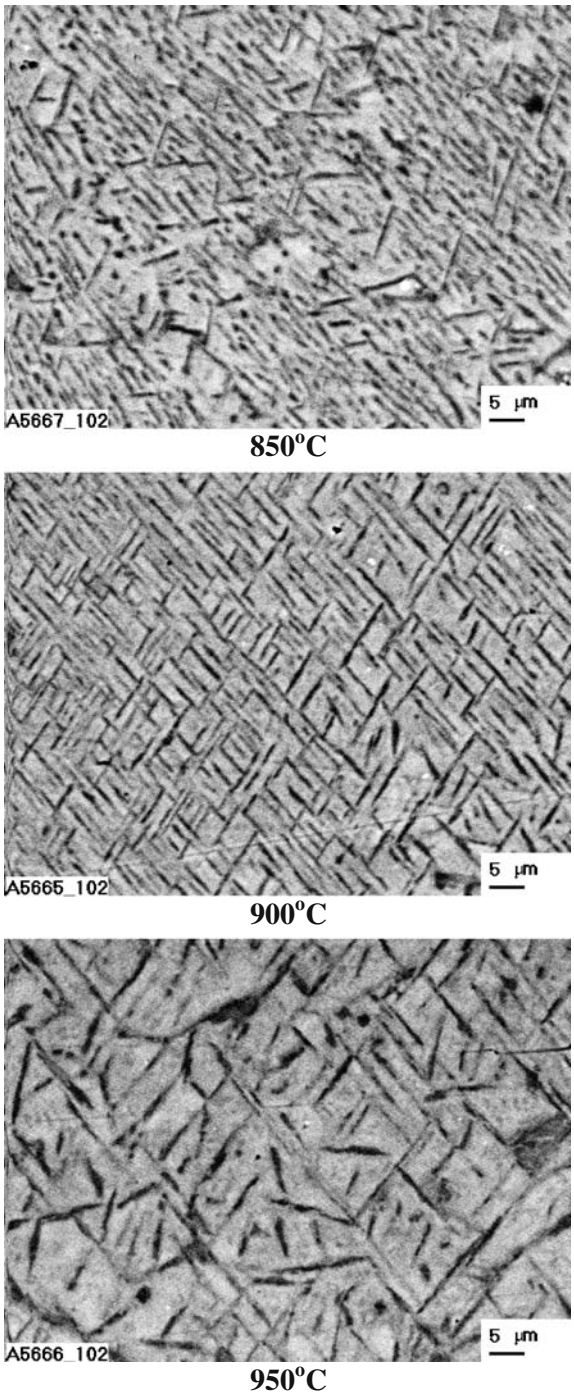

Fig. 5 Plain-view micrographs corresponding to section I in Fig. 2. The brighter regions are the FeB phase enriched in iron, while the darker regions are the FeB phase enriched in chromium

of k_{outer} and k_{inner} was estimated from the densities of the FeB and Fe_2B compounds (6.706×10^3 kg m^{-3} and 7.336×10^3 kg m^{-3}, respectively [1]) as 0.60. The derivatives were found from the experimental layer thickness-time dependences by the numerical three-point method.

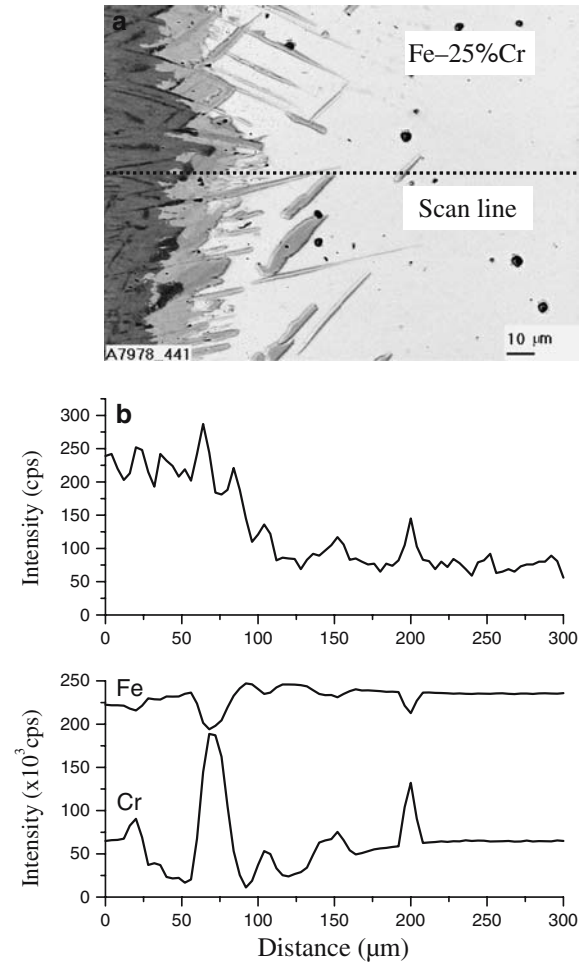

Fig. 6 Microstructure of the transition zone between an Fe–25% Cr alloy and boron and concentration profiles of Fe, Cr and B. Boriding conditions: temperature 950 °C, reaction time 21600 s (6 h)

As seen from Table 5, the results of calculations using the system of equations 1 are strongly dependent upon the accuracy of measuring layer thicknesses. Approximations of experimental data with any suitable analytical functions are therefore advisable to obtain more accurate values of k_{outer} and k_{inner}. For example, the use of parabolic relations to approximate the layer thickness–time dependences and then to find the derivatives produces another set of values of k_{outer} and k_{inner} (Table 6). Comparing these with the average values of k_{outer} and k_{inner} found numerically from the experimental points, it may be concluded that both sets of the constants agree fairly well, providing evidence for the validity of the analytical treatment proposed.

As seen from Fig. 10, the temperature dependence of the layer growth-rate constants is described in the 850–950 °C range by a relation of the Arrhenius type

$$K = A \exp(-E/RT) \quad (2)$$

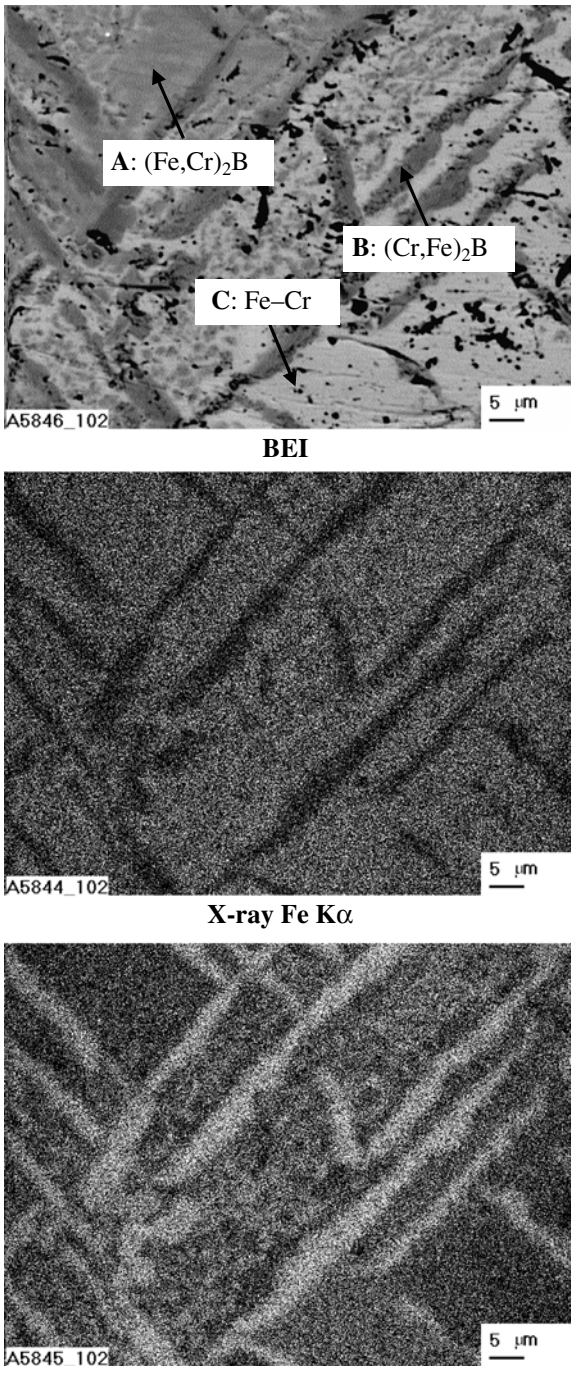

Fig. 7 Plain-view micrograph corresponding to section III in Fig. 2 and X-ray maps for iron and chromium (the brighter the region, the higher is the content of an appropriate element). BEI = backscattered electron image

where K stands for any constant, A is the frequency factor, E is the activation energy, R is the gas constant and T is the absolute temperature. Application of the least squares fit method yields the following equations:

$$k_1 = 1.86 \times 10^{-8} \exp(-130.2\,\mathrm{kJ\,mol^{-1}}/RT)\,\mathrm{m^2\,s^{-1}}$$
for the FeB layer,

$$k_1 = 3.27 \times 10^{-9} \exp(-118.0\,\mathrm{kJ\,mol^{-1}}/RT)\,\mathrm{m^2\,s^{-1}}$$
for the Fe2B layer,

$$k_1 = 3.74 \times 10^{-8} \exp(-125.9\,\mathrm{kJ\,mol^{-1}}/RT)\,\mathrm{m^2\,s^{-1}}$$
for both boride layers,

$$k_{\mathrm{outer}} = 8.07 \times 10^{-8} \exp(-128.3\,\mathrm{kJ\,mol^{-1}}/RT)\,\mathrm{m^2\,s^{-1}},$$

$$k_{\mathrm{inner}} = 4.32 \times 10^{-8} \exp(-121.7\,\mathrm{kJ\,mol^{-1}}/RT)\,\mathrm{m^2\,s^{-1}}.$$

Degradation of boride layers during annealing in the absence of boriding media

Annealing of a borided Fe–Cr sample (Fig. 11a) in the absence of boriding media results in a decrease of the thickness of the FeB layer and an appropriate increase of the thickness of the Fe_2B layer. As seen in Fig. 11b and c, the FeB layer, initially compact and around 40 μm thick, disintegrates into separate grains during annealing at 950 °C and after a 12-h hold disappears almost completely as a result of the chemical reaction between iron and FeB to form Fe_2B.

This type of consumption is characteristic of non-homogeneous layers. Homogeneous layers are usually consumed as a whole at their interface with an adjacent layer, with their compactness retaining and their thickness decreasing. The first phase to disappear is seen in Fig. 11b and c to be (Fe,Cr)B because the remaining crystals of the outer (Fe,Cr)B–(Cr,Fe)B layer are black. This is confirmed by EPMA measurements. The chemical composition of black crystals of the outer (Fe,Cr)B–(Cr,Fe)B layer in Fig. 11c is 50 ± 2 at.% B, 17 ± 3 at.% Fe and 33 ± 4 at.% Cr. Wherever remained between black crystals, the (Fe,Cr)B phase has a composition of 50 ± 2 at.% B, 35 ± 3 at.% Fe and 15 ± 3 at.% Cr. Darker crystals of the outer (Fe,Cr)B–(Cr,Fe)B layer have a composition of 33 ± 2 at.% B, 22 ± 5 at.% Fe and 45 ± 5 at.% Cr. Brighter crystals of this layer contain 33 ± 2 at.% B, 25 ± 3 at.% Fe and 42 ± 3 at.% Cr.

It should be noted that elongated crystals of the $(Cr,Fe)_2B$ phase penetrating deep into the alloy base actually do not grow in the absence of boriding media

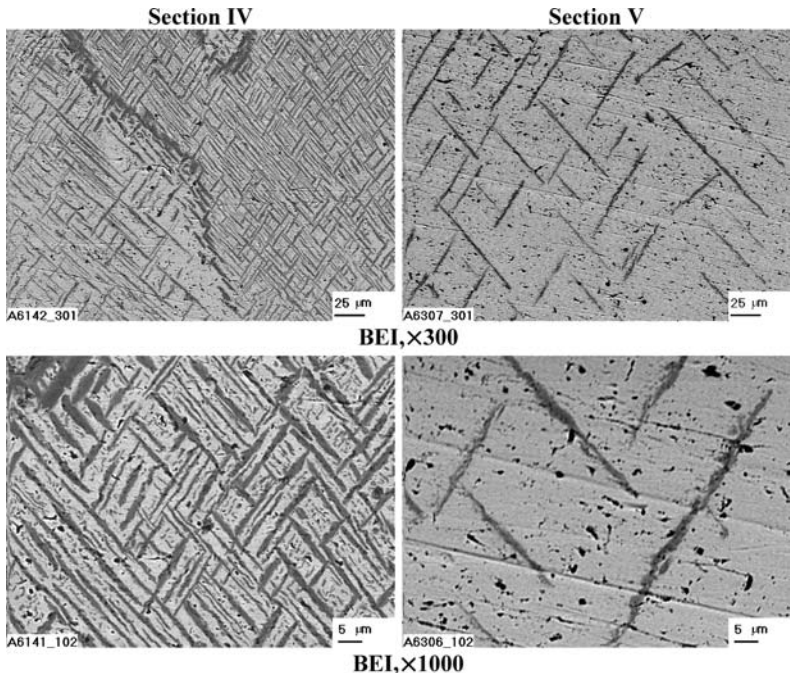

Fig. 8 Plain-view micrographs corresponding to sections IV and V in Fig. 2. The darker regions are the $(Cr,Fe)_2B$ phase, while brighter regions are the Fe–Cr alloy base. Black spots are holes and cracks. BEI = backscattered electron image. Magnification: ×300 and ×1000

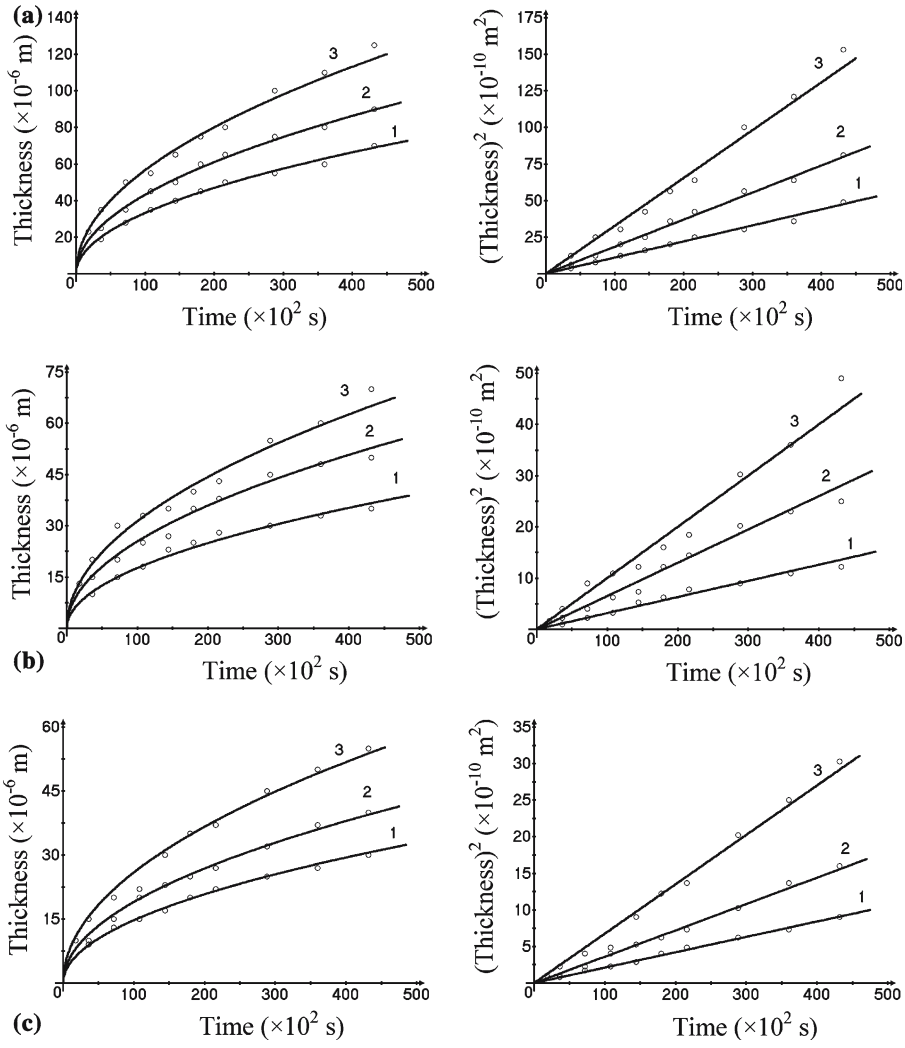

Fig. 9 Plots of layer thickness (left) and squared layer thickness (right) against time for (**a**) both boride layers, (**b**) the FeB layer and (**c**) the Fe_2B layer formed at the Fe–25% Cr alloy–boron interface at a temperature of 850 °C (line 1), 900 °C (line 2) and 950 °C (line 3)

Table 5 Kinetic data for the boride layers formed at the Fe–25% Cr alloy-boron interface

Temperature (°C)	Time ($\times 10^2$ s)	x($\times 10^{-6}$ m)				k_1($\times 10^{-14}$ m^2 s^{-1})		k($\times 10^{-13}$ m^2 s^{-1})	
		Total	FeB	Fe_2B	Total	FeB	Fe_2B	k_{outer}	k_{inner}
850	36	19	10	9	5.0	1.4	1.1		
	72	28	15	13	5.1	1.6	1.2	1.3	1.6
	108	33	18	15	5.0	1.5	1.0	0.93	1.0
	144	40	23	17	5.5	1.8	1.0	1.1	1.1
	180	45	25	20	5.6	1.7	1.1	0.99	1.1
	216	50	28	22	5.7	1.8	1.1	0.85	0.91
	288	55	30	25	5.3	1.6	1.1	0.60	0.68
	360	60	33	27	5.0	1.5	1.0	0.66	0.74
	432	65	35	30	5.7	1.4	1.0		
900	36	25	15	10	8.7	3.1	1.4		
	72	35	20	15	8.5	2.8	1.6	1.6	1.6
	108	45	25	20	9.4	2.9	1.9	1.5	1.6
	144	50	27	23	6.9	2.5	1.8	1.7	1.9
	180	60	35	25	8.3	3.4	1.7	2.3	2.1
	216	65	38	27	9.8	3.3	1.7	1.6	1.5
	288	75	45	30	9.8	3.5	1.7	1.8	1.6
	360	80	48	37	8.9	3.2	1.9	1.3	1.5
	432	90	50	40	9.4	2.9	1.9		
950	18	23	13	10	14.6	4.7	2.8		
	36	35	20	15	17.0	5.6	3.1	3.3	3.3
	72	50	30	20	17.4	6.2	2.8	2.6	2.2
	108	55	33	22	14.0	5.0	2.2	1.8	1.8
	144	65	35	30	14.7	4.3	3.1	2.6	3.2
	180	75	40	35	15.6	4.4	3.4	2.4	2.9
	216	80	43	37	14.8	4.2	3.2	2.7	3.1
	288	100	55	45	17.4	5.3	3.5	3.4	3.7
	360	110	60	50	16.8	5.0	3.5	1.2	1.4
	432	125	70	55	18.1	5.7	3.5		

(B+KBF_4). The boron atoms released at the interface between two boride layers, then diffuse across the Fe_2B layer and react with iron from the alloy base to form more Fe_2B at the Fe_2B–alloy interface. The thinner the Fe_2B layer at a certain place, the shorter is the diffusion path and hence the higher is the supply of diffusing boron atoms to that place. Therefore, at thinner places the growth rate of the Fe_2B layer is higher than at thicker ones. As a result, the Fe_2B–alloy interface flattens with passing time, as evidenced in Fig. 11b and c.

Table 6 Average values of layer growth-rate constants

Temperature (°C)	k_1 ($\times 10^{-14}$ m^2 s^{-1})			k ($\times 10^{-13}$ m^2 s^{-1}) from experimental points		k ($\times 10^{-13}$ m^2 s^{-1}) from approximated dependences	
	Total	FeB	Fe_2B	k_{outer}	k_{inner}	k_{outer}	k_{inner}
850	5.3	1.6	1.1	0.92	1.02	0.86	0.96
900	8.9	3.1	1.7	1.69	1.71	1.60	1.59
950	16.0	5.0	3.1	2.49	2.69	2.63	2.79

These experiments clearly show the essential, if not decisive, role of diffusion of a gaseous boron-containing phase, probably BF_3 [1, 8, 18], in the course of boriding of Fe–Cr alloy samples in a mixture of B and KBF_4 under reduced pressure. Defects of a certain kind and probably some solid-state transformation in the alloy base, providing

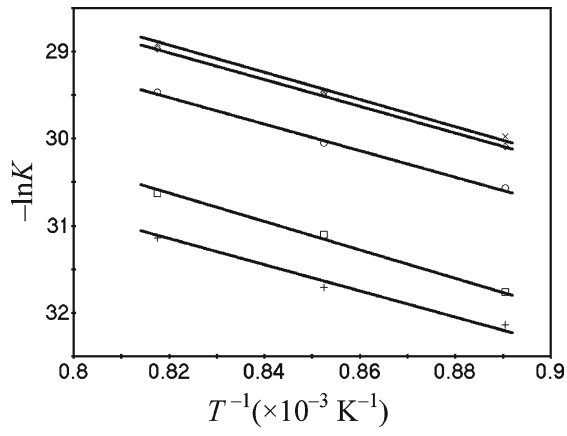

Fig. 10 The temperature dependence of the layer growth-rate constants K: ×, k_{inner}; ◇, k_{outer}; ○, k_1 for both boride layers; □, k_1 for FeB; +, k_1 for Fe_2B

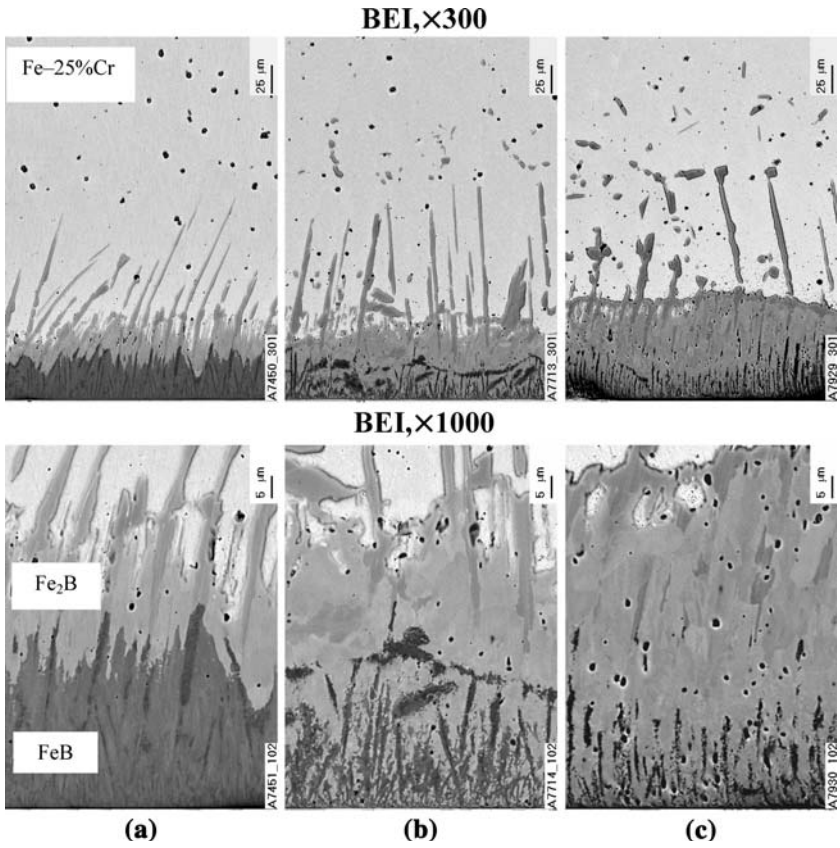

Fig. 11 Degradation of boride layers during vacuum annealing at a temperature of 950 °C in the absence of boriding media: (**a**) as-received condition, (**b**) 6 h annealing and (**c**) 12 h annealing. BEI = backscattered electron image. Magnification: ×300 and ×1000

Table 7 Results of abrasive wear resistance tests of borided Fe–Cr alloy samples. Boriding conditions: temperature 950 °C, reaction time 21600 s (6 h)

Borided sample number	Test number	Δm (g)[a]	r*	Δh (mm)	Phase
111	1	0.00190	154	~0.01	(Fe,Cr)B–(Cr,Fe)B
	2	0.00095	307	< 0.01	(Fe,Cr)B–(Cr,Fe)B
112	1	0.00195	150	~0.01	(Fe,Cr)B–(Cr,Fe)B
	2	0.00085	344	< 0.01	(Fe,Cr)B–(Cr,Fe)B
113	1	0.00200	146	~0.01	(Fe,Cr)B–(Cr,Fe)B
	2	0.00085	344	< 0.01	(Fe,Cr)B–(Cr,Fe)B
		0.29200	1	0.36	Non-borided sample

*r is an increase in wear resistance in comparison with the alloy base

[a]Δm and Δh are changes in mass and height, respectively, of tablet samples

the paths of rapid diffusion for the gaseous boriding agent, are responsible for the deep penetration of the $(Cr,Fe)_2B$ crystals into the sample bulk. It can hardly be solely a result of the peculiarities of the Fe_2B crystal structure, as is usually explained [1]. The regular arrangement of the constituting phases in both boride layers provides evidence for an additional solid-state transformation. It may either take place simultaneously with the layer growth or precede or follow it. This transformation may be closely connected with the occurrence of hot cracks that boron (>0.007%) is known to cause in steels at elevated temperatures [19].

Abrasive wear resistance of boride layers

Boriding the Fe–Cr alloy tablets for abrasive wear resistance tests was performed at 950 °C for 6 h, producing the (Fe,Cr)B–(Cr,Fe)B and $(Fe,Cr)_2B$–$(Cr,Fe)_2B$ layers of approximately equal thickness (around 80 μm in total). Two consecutive tests were carried out on each borided Fe–Cr sample, with each test along a fresh track on emery paper. The results obtained are presented in Table 7, where the data for a non-borided Fe–Cr sample are also given for comparison.

The wear resistance of the (Fe,Cr)B–(Cr,Fe)B layer, found from mass loss measurements, proved to be 150 (outermost portions) to 350 (deeper portions) times greater than that of the alloy base. Somewhat lesser resistance of its outermost portions, compared to deeper ones, is due to both the greater amount of cracks in the near-surface region and a lesser orientation order and hence the compactness of the boride phase.

Even though chromium is known to increase the abrasive wear resistance of steels [1, 18], in the present case the extent of its influence appears to be unexpectedly high. Unlike a Fe–10% Cr alloy, with which three consecutive tests on each sample were sufficient to reach the alloy base [20], it was impossible to do the same with Fe–25% Cr alloy samples, carrying out a reasonable amount of consecutive tests.

Most probably, the great gain in wear resistance of a Fe–25% Cr alloy is due to structural (or morphological) rather than compositional reasons. Further investigations with the use of additional experimental techniques are needed to fully explain this effect.

Conclusions

Two boride layers based on the FeB and Fe_2B compounds are formed at the interface between a Fe–25% Cr alloy and boron at 850–950 °C and reaction times up to 12 h. The characteristic feature of both layers is a pronounced texture. The strongest reflections are {002} and {020} for the orthorhombic FeB phase and {002} for the tetragonal Fe_2B phase.

Each of two boride layers is compositionally two-phase. The outer layer consists of the (Fe,Cr)B and (Cr,Fe)B phases. The inner layer comprises the $(Fe,Cr)_2B$ and $(Cr,Fe)_2B$ phases.

Growth kinetics of boride layers is close to parabolic. Alternatively, layer-growth kinetics can be described by a system of non-linear differential equations, also producing a fairly good fit to the experimental data.

Annealing of a borided Fe–Cr sample in the absence of boriding media results in the disappearance of the (Fe,Cr)B–(Cr,Fe)B layer, with the (Fe,Cr)B phase disappearing first.

Microhardness values are 21.0 ± 2.0 GPa for the outer (Fe,Cr)B–(Cr,Fe)B layer, 18.0 ± 1.0 GPa for the inner $(Fe,Cr)_2B$–$(Cr,Fe)_2B$ layer and 1.35 ± 0.09 GPa for the Fe–25% Cr alloy base.

The abrasive wear resistance of the (Fe,Cr)B–(Cr,Fe)B layer, found from mass loss measurements, is 150 (outermost portions) to 350 (deeper portions) times greater than that of the alloy base.

Acknowledgments This investigation was supported in part by the STCU grant No. 2028. The authors thank V.G. Khoruzha, V.R. Sidorko, K.A. Meleshevich and A.V. Samelyuk for their help in conducting the experiments and carrying out the necessary analyses.

References

1. Voroshnin LG, Lyakhovich LS (1978) Borirovaniye stali. Metallurgiya, Moskwa (in Russian)
2. Kunst H, Schroll H, Luetje R, Wittel K, Lugscheider E, Weber T, Eschnauer HR, Raub C (1991) In: Ullmann's Encyclopedia of Industrial, vol A16. Chemistry Verlag Chemie, Weinheim, p 427
3. Sinha AK (1982) In: Sinha AK (ed) Metals handbook, ASM International, Metals Park, OH, p 844
4. Hansen M (1958) Constitution of binary alloys, 2nd edn. McGraw-Hill, New-York, p 249
5. Vol AE (1962) Stroeniye i svoystva dvoynikh metallicheskikh system, vol 1, Fizmatgiz, Moskwa, p 679 (in Russian)
6. Massalski TB, Murray JL, Bennett LH, Baker H (1986) Binary Alloy Phase Diagrams, vol. 1. American Society of Metals, Metals Park, OH, p 351
7. Okamoto H (2004) J Phase Equilibria Diffusion 25:297
8. Brandstötter J, Lengauer W (1997) J Alloys Compd 262–263:390
9. Gurov KP, Kartashkin BA, Ugaste Yu A (1981) Vzaimnaya diffusiya v mnogofaznikh metallicheskikh sistemakh. Nauka, Moskwa (in Russian)
10. Dybkov VI (2002) Reaction diffusion and solid state chemical kinetics (The IPMS Publications, Kyiv) (available for reading at http://www.i.com.ua/~dybkov/V)
11. Gorelik SS, Rastorguev LN, Skakov Yu A (1970) Rentgenograficheskiy i elektronno-opticheskiy analiz, prilozheniya. Metallurgiya, Moskwa, p 29 (in Russian)
12. Goeuriot P, Fillit R, Thevenot F, Driver JH, Bruyas H (1982) Mater Sci Eng 55:9
13. Carbucicchio M, Palombarini G (1987) J Mater Sci Lett 6:1147–1149
14. Martini C, Palombarini G, Carbucicchio M (2004) J Mater Sci 39:933
15. Seith W (1955) Diffusion in metallen. Springer, Berlin
16. Hauffe K (1955) Reaktionen in und an festen Stoffen Springer, Berlin
17. Dybkov OV, Dybkov VI (2004) J Mater Sci Lett 39:6615–6617
18. Voroshnin LG (1981) Borirovaniye promyshlennikh staley i chugunov. Belarus, Minsk (in Russian)
19. Motovilin GV, Masino MA, Suvorov OM (1989) Avtomobilnie materialy. Transport, Moskwa (in Russian)
20. Dybkov VI, Lengauer W, Barmak K (2005) In: Proc 16th Plansee Seminar, Reutte, Austria, May 31–June 4, vol 2, pp 999–1009